International Journal of Mechanical Sciences 209 (2021) 106699

Contents lists available at ScienceDirect

International Journal of Mechanical Sciences

journal homepage: www.elsevier.com/locate/ijmecsci

A 3D Mechanism-driven Hexagonal Metamaterial: Evaluation of Auxetic Behavior

Yutai Su [a], Xianchen Xu [b], Jing Shi [a,*], Guoliang Huang [b]

[a] Department of Mechanical & Materials Engineering, College of Engineering and Applied Science, University of Cincinnati, Cincinnati, OH 45221, USA
[b] Department of Mechanical & Aerospace Engineering, University of Missouri, Columbia, MO 65211, USA

ARTICLE INFO

Keywords:
Sliding mechanism
metamaterial
auxetic behavior
re-entrant structure
friction coefficient
finite element simulation

ABSTRACT

This paper investigates an unconventional 3D printable auxetic metamaterial realized by a unique sliding mechanism. The concept of 3D sliding induced hexagonal auxetic (SIHA) metamaterial is proposed with stable auxetic behavior and improved compression load response, as compared with the conventional re-entrant structure. For a single SIHA lattice cell, the theoretical model concerning the sliding mechanism is developed and verified by both finite element analysis (FEA) and experiment. Furthermore, the compression properties of the periodic SIHA structure are evaluated by FEA with experimental verification. A 3D conventional re-entrant honeycomb (REH) structure is adopted for comparison. It is shown that the FEA results agree with the experimental results, and overall superior performance of SIHA structure is obtained, which is reflected by higher compression resistance and more stable auxetic behavior. Moreover, the sensitivity of performance with respect to the friction coefficient in the sliding mechanism is investigated. It is found that the performance and auxetic behavior of the SIHA metamaterial is sensitive to the friction condition. Force-strain curve increases with the input friction coefficient, while an excessive friction coefficient may cause undesirable effects on the slip mechanism. Overall, the friction sliding and collapsing structural mechanism-driven structures could provide a new way to entrap elastic energy under compression deformations.

1. Introduction

Metamaterials are artificial structures or composite materials with extraordinary physical properties that can overcome the limitations of natural materials [1-3], and research has shown numerous novel applications of metamaterials such as energy absorbers [4,5], negative refractive indices [6,7], cloaking [8,9], and superlens [10]. Mechanical metamaterials, a major category of metamaterials, have attracted tremendous research interests thanks to the unconventional performance, the advancement in fabrication techniques, and the increasing needs in industrial and commercial applications [11-13]. A significant fraction of research on mechanical metamaterials is focused on auxetic behavior, which means the materials have a negative Poisson's ratio. The auxetic metamaterials become thinner under uniaxial compression and wider under uniaxial tension, which was first discovered by Lakes [14]. The unique behavior has opened up numerous new possibilities, such as the combination of superior mechanical properties with significant weight reduction in applications.

The study of auxetic metamaterials can be traced back to the proposed re-entrant honeycomb structure by Gibson et al. [15] and Masters et al. [16]. Thereafter, the research for auxetic metamaterial has bloomed and many other mechanisms have been proposed. Meanwhile, because of the favorable impact energy absorption ability of auxetic metamaterials, the mechanical behaviors of auxetic metamaterials under high strain rates have attracted increasing attention [17-19]. To this end, researchers have investigated many auxetic structures that have superior mechanical properties to meet the performance requirement. For many years, the new structure design of an auxetic metamaterial is largely based on the designed local deformation of hinges interacting with the rest of the structure to achieve auxetic behavior [20-24]. Therefore, most of the new auxetic metamaterials based on local deformation are constructed by a single piece unit cell. The Poisson's ratio will mostly increase during the deformation. Moreover, the auxtetic behavior of the conventional design is largely affected by the materials used to construct the structure, because the deformation strategy involves the rotation of the structural frame connected to the hinges. The higher the material stiffness, the higher the Poisson's ratio of the conventional structures [24-29]. Recently, some studies have reported novel mechanisms containing separate moving parts within the auxetic cell that can help improve the mechanical properties compared to the conventional auxetic metamaterials [30-32]. For example, Kim et al. [30] proposed a numerical model for auxetic metamaterials with rigid sliding units. It was shown that the auxetic behavior of rigid sliding metamaterials can be theoretically kept at a constant negative value and the deformation mechanisms do not involve the rotation of structure which gives the freedom to choose the different materials and eliminate the influence

* Corresponding author.
E-mail address: jing.shi@uc.edu (J. Shi).

https://doi.org/10.1016/j.ijmecsci.2021.106699
Received 2 May 2021; Received in revised form 27 July 2021; Accepted 27 July 2021
Available online 2 August 2021

on the auxetic performance. The proposed design can create a stable superior mechanical property under the uniaxial compression load. With further investigation, the concept of achieving auxetic behavior by separate sliding units might lead to the development of a new field for auxetic metamaterials [31].

This paper reflects our effort to design a new auxetic metamaterial with the sliding mechanism, in which the hexagonal profile is considered to achieve superior uniaxial mechanical properties. The hexagonal geometries adapted from the natural structure are often used in other types of metamaterials because of their excellent mechanical properties under the uniaxial compression load [33, 34]. Certainly, the exceptional mechanical properties of the hexagonal structure are not limited to metamaterials, which are widely reported by researchers [39-43]. In this study, a solid hexagonal column is used to design the auxetic unit cell. The hexagonal column is divided, expanded, and separated into a larger hollow hexagonal unit cell with multiple sliding units. The sliding units are expected to slide along the sliding surface and shrink the larger hexagonal unit cell back to its original shape under the compression load to create the auxetic behavior. In the study, we demonstrate the effectiveness of the auxetic metamaterial for both a single cell and a periodic structure by simulation and experiment approaches.

2. Mechanism of Hexagonal Auxetic Metamaterial

As mention previously, auxetic metamaterials are promising lightweight materials with numerous applications such as energy-absorbing due to their unique behaviors of horizontal contraction under uniaxial compression loading, which is conventionally realized by the strut-hinges interaction of the structure [20-24]. However, in the study, the auxetic behavior is realized by the conversion of uniaxial load to horizontal strain by sliding mechanism. In the research of thin wall energy absorbers, the inversion is commonly used as a dissipation mechanism which involves transferring the uniaxial load to the horizontal load by a designed slop structure [35-37]. For instance, Gao et al. [38] proposed a splitting circular thin wall structure for energy absorption by using a cone-shaped die to scatter the uniaxial impact loading to the structure in the horizontal direction. The similar mechanism is used to design the unit cell of SIHA structure in this study, which also attempts to convert the uniaxial load to the horizontal strain. The design strategy is to create a sliding surface within the SIHA unit cell to achieve auxetic behavior and convert the uniaxial compression load. The detailed geometry model is presented in the following along with the mechanical analysis of the SIHA unit cell.

2.1. Design methodology

The SIHA structure is designed by adapting the mechanism containing sliding units and the hexagonal shape profile due to the unique ability to maintain the negative Poisson's ratio with the various stages of uniaxial strain and excellent mechanical capacity under compression loads. It should be stressed that, unlike the conventional metamaterials with negative Poisson's ratio [20-24], the auxetic deformation of the proposed SIHA structure is mainly driven by the internal collapsing mechanism, and the SIHA metamaterials are designed for enduring compression load exclusively. The sliding mechanism would not be suitable for tensile loading in that the sliding units must contact the hexagonal ring to initiate the sliding interaction, which only occurs when the SIHA structure endures compression load.

The basic sketch for elaborating the design methodology to achieve the auxetic behavior is shown in Fig. 1. The concept is about contracting a large hexagonal unit (see in Fig. 1 (a)) into a smaller unit cell (see in Fig. 1 (b)) under compression load along the z-direction. Hence, the cake-like sliding units (the red part in Fig. 1 (a)) slipped in the honeycomb ring (the green part in Fig. 1 (a)) will match the external dimension of the smaller hexagonal unit under the compression load, which is similar to auxetic behavior. To achieve this mechanism, an inverse procedure is used to design the pattern which starts from the deformed unit cell in Fig. 1 (b), and expands to the undeformed structure in Fig. 1 (a) by adding connections between the cake-like sliding units. It can be seen that a solid hexagonal column is divided into twelve individual cake-like bulk units which act as sliding units, as well as a hexagonal ring which is similar to a single honeycomb cell. As a result, the twelve individual sliding units expand along the cutting surface against the hexagonal ring to establish an auxetic hexagonal column unit cell in Fig. 1 (a).

To analyze the influence of dimensional parameters on auxetic behavior, we focus on the 2-D cross-sectional sketch along x-direction as shown in Fig. 1 (c). As the axial compression load is applied to the structure, the sliding units then move along the sliding surface. When the unit cell deforms uniformly under the compression load from the expend shape, the horizontal direction ΔL_x and axial direction ΔL_z can be defined as

$$\Delta L_x = 2d\cos\theta \tag{1}$$

$$\Delta L_z = 2d\sin\theta \tag{2}$$

L_x and L_z can be expressed as

$$L_x = l_x + 2\,d\cos\theta \tag{3}$$

$$L_z = l_z + 2\,d\sin\theta \tag{4}$$

Where d is the total sliding distance of sliding units, and θ is the angle of the sliding surface, L_x and L_z are the original horizontal length and axial height of the auxetic hexagonal column, l_x and l_z are the horizontal length and axial height after deformation, respectively.

2.2. Connected assembly

The single unit cell as shown in Fig. 1 consists of separate individual parts. To eliminate the need of component assembly, the separate parts should be connected in the design so that the connected structure can be made at once without difficulty via 3D printing. As such, additional structures must be introduced to the SIHA unit cell. The requirements of additional connection structures are as follows. (1) The connection structure should link the sliding units shown in Fig. 1 (the red regions). (2) The connection structure should also link the sliding units and hexagonal ring shown in Fig. 1 (the red and green regions). (3) The collapsing and buckling forces of the connection structure during the compression test should create minimum influence on the sliding mechanism and promote the sliding force between the sliding units and hexagonal ring simultaneously. As a result, the V-shaped connectors, columnar connection structures, and extended height are introduced into the SIHA unit cell.

First, the V-shaped connectors (i.e., the green regions shown in Fig. 2(a)) are added to connect the individual sliding units (i.e., the gray regions in Fig. 2(a)). The V-shaped connectors are expected to fold into the reserved spaces during the compression to minimize influence on the sliding mechanism and provide the elastic energy against the sliding surface to increase the friction force to the SIHA structure. The height and thickness of the V-shaped connectors are 3 mm and 1 mm. Then, the yellow regions shown in Fig 2(a) are the extensions from the sliding units to connect SIHA units, and the thickness of the extensions is 1 mm. Finally, the red regions in Fig. 2 (b) show the connection structures to connect the hexagonal ring (i.e., the transparent region in Fig. 2(b)) and the sliding units. The height, width, and thickness of the connection structure are 4.5 mm, 2 mm, and 1 mm, respectively. The dimensions of the connectors were chosen to be small and yet ensure reasonably consistency in part quality, under the resolution constraint of our digital light processing (DLP) 3D printer. Note that if a higher resolution printer were to be available, the connector dimensions could be further reduced.

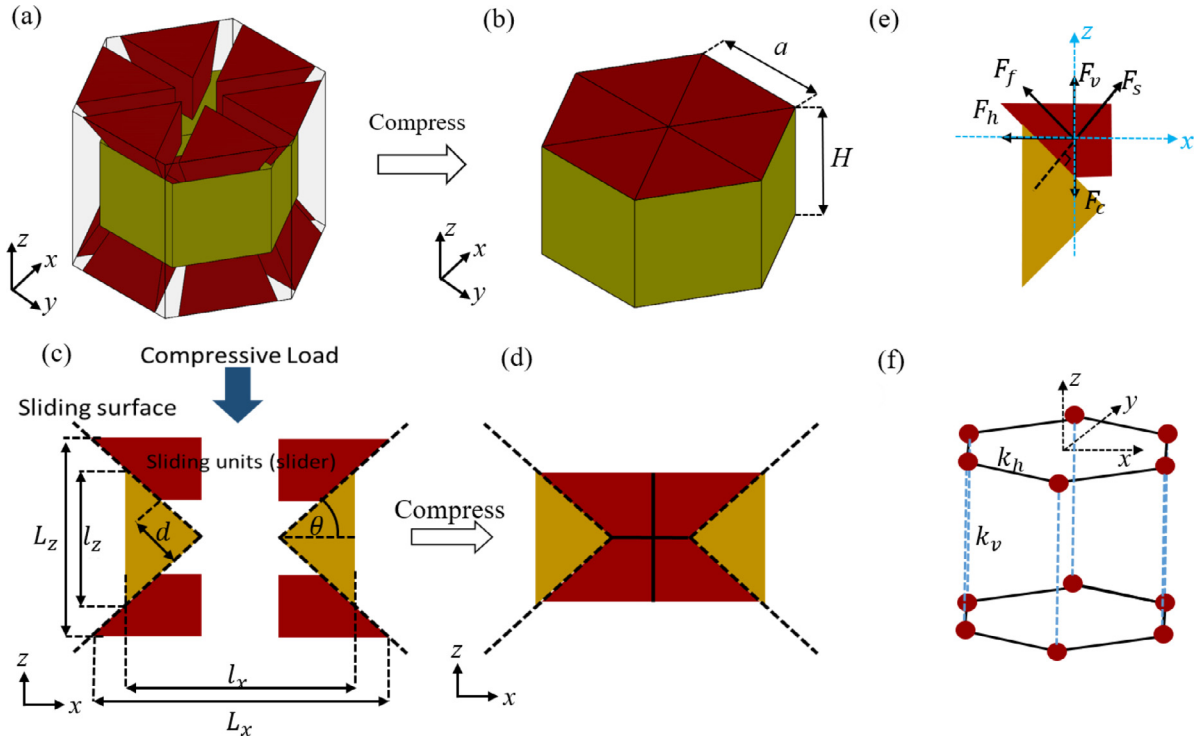

Fig. 1. The concept design of a SIHA metamaterial, (a) an undeformed hexagonal column, (b) a deformed hexagonal column, (c) the undeformed cross-section view of the auxetic hexagonal column, (d) the deformed cross-section view of the auxetic hexagonal column, (e) the force diagram of the deformed hexagonal column, and (f) the effective model of the hexagonal column.

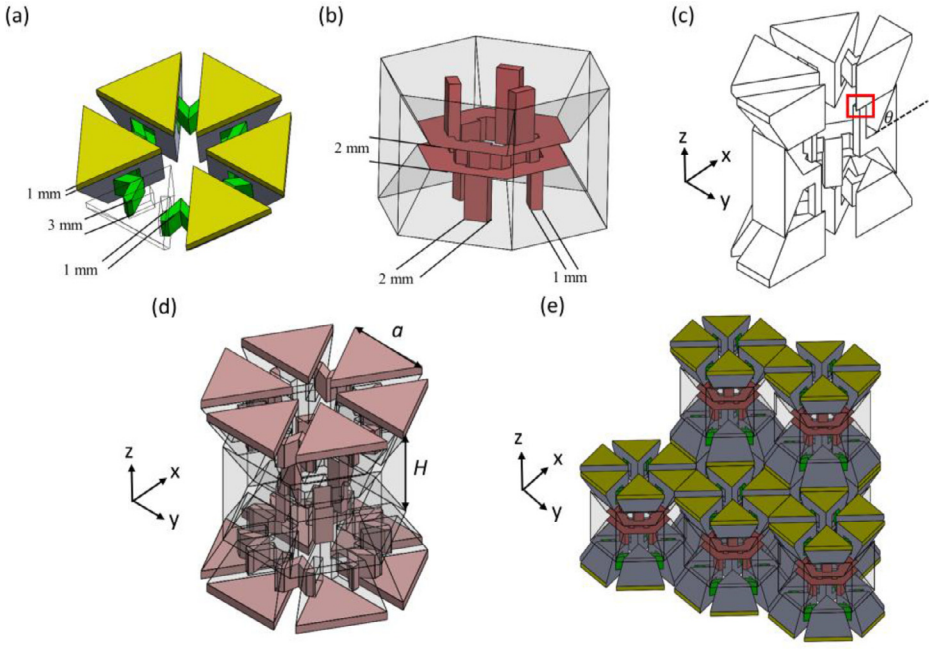

Fig. 2. Schematics of auxetic hexagonal column unit cell, (a) sliders with V-shaped connectors (green regions) and extensions (yellow regions), (b) grouped structure of hexagonal ring and connection structures, (c) cross-sectional view of a single SIHA unit cell, (d) illustration of connection structures (highlighted regions) in a unit cell, and (e) illustration of the formation of the SIHA periodic model.

In general, the connectors in Fig. 2(a) link the individual sliding units, and the connection structure in Fig. 2(b) links the connected sliding units at the top and the bottom with the hexagonal ring, and the connection can be seen at the tips of sliding units as shown in Fig. 2(c) (highlighted area). The assembled structure leads to a single SIHA unit cell shown in Fig. 2(c) or Fig. 2(d). The packing factor of the SIHA unit cell is 30%. The formation of the SIHA periodic model is accomplished by connecting the extension layers (the yellow regions in Fig. 2(a)) of the individual SIHA unit cells, and the resultant periodic SIHA structure is illustrated in Fig. 2(e).

2.3. Mechanical analysis for single SIHA cell

Recall that the auxetic hexagonal column is expanded from a solid hexagonal column, l_x and l_z are equal to $\sqrt{3}a$ and H respectively, where H is the height and a is the side length of the compressed hexagonal col-

umn as shown in Fig. 1 (d). Thus, the strains of the horizontal direction ε_x and axial direction ε_z can be written as

$$\varepsilon_x = \frac{2d\cos\theta}{\sqrt{3}a + 2d\ cos\theta} \tag{5}$$

$$\varepsilon_z = \frac{2d\sin\theta}{H + 2d\sin\theta} \tag{6}$$

Poisson's ratio v, which is defined as the negative ratio of the horizontal strain and axial strain, is given by [16],

$$v = -\frac{\varepsilon_x}{\varepsilon_z} = -\frac{H\cos\theta + 2d\sin\theta\cos\theta}{\sqrt{3}a\sin\theta + 2d\sin\theta\cos\theta} \tag{7}$$

It can be seen that the relationship between the Poisson's ratio and physical geometry is simplified to four major dimensional parameters where the range of θ is $0 < \theta < \frac{\pi}{2}$.

Hexahedral crystals in Fig 1 (e) may show some structural degeneracy. This means that structures other than that shown in Fig 1 (a), but of the same connection per molecule, can be formed by the spring connection. As shown in Fig. 1 (e), the compression on auxetic hexagonal metamaterials can be regarded as a quasi-static process, and Newton's first law should be considered. The whole structure will satisfy the following equations:

$$F_c = F_{sz} + F_v + F_{fz} \tag{8}$$

$$F_{sx} = F_{fx} + F_h \tag{9}$$

Where F_c, F_s, F_v, F_f, and F_h are compression force, reaction force at support, vertical force contributed by the vertical connection between sliding units, friction force, and horizontal force contributed by the in-plane connection between sliding units, respectively. Also, x and z are the directional component subscripts along x and z directions, respectively. The force components have the following relations,

$$F_{sz} = F_s\cos\theta,\ F_{sx} = F_s\sin\theta, F_{fz} = F_f\sin\theta,\ F_{fx} = F_f\cos\theta \tag{10}$$

Considering the Amontons' first law, the relation between friction force and reaction force at support can be expressed as

$$F_f = \mu F_s \tag{11}$$

Substitute Eqs. (10) and (11) into Eqs. (8) and (9), we have

$$F_c = \frac{F_h}{(\sin\theta - \mu\cos\theta)}(\cos\theta + \mu\sin\theta) + F_v \tag{12}$$

As shown in Fig. 1(f) and Fig. 2 (d), the additional connection is expected to provide the collapsing force against the sliding units and enhance the friction force on the sliding surface. When the hexagonal column is under uniaxial compression, the support structures will shrink because the sliding units will slide into the hexagonal ring as shown in Fig. 1(c)-(d), then the buckling and collapsing of the support connection will provide extra collapsing force to the sliding units which will create the additional friction force at the sliding surface. Therefore, the combination of sliding and collapsing mechanisms can trap large uniaxial mechanical deformations by horizontal collapsing force. Based on the design, the connection between the sliding units in the same plane can be simplified as a horizontal spring k_h, and the connection between two sliding units in the different plane can be simplified as a vertical spring k_v. To obtain the accurate values of the spring constants, the values of k_h and k_v are obtained by fitting the experimental compression curve of the unit cell, which is to be described in the next section.

Therefore, the horizontal force and the vertical support force can be expressed as

$$F_h = k_h d\cos\theta \tag{13}$$

$$F_v = k_v d\sin\theta \tag{14}$$

where k_h and k_v are the horizontal and vertical spring constants between the sliding units. Thus, the relation between compression and sliding can be expressed as

$$F_c = \frac{k_h d\cos\theta}{(\sin\theta - \mu\cos\theta)}(\cos\theta + \mu\sin\theta) + k_v d\sin\theta \tag{15}$$

Substitute Eqs. (5) and (6) into Eq. (15), the relation between compression and horizontal strain and axial strain can be expressed as

$$F_{cx} = k_h\frac{\sqrt{3}a\varepsilon_x(\cos\theta + \mu\sin\theta)}{2(\sin\theta - \mu\cos\theta)(1-\varepsilon_x)} + k_v\frac{\sqrt{3}a\varepsilon_x\sin\theta}{2\cos\theta(1-\varepsilon_x)} \tag{16}$$

$$F_{cz} = k_h\frac{H\varepsilon_z(\cos\theta + \mu\sin\theta)}{2\sin\theta(\sin\theta - \mu\cos\theta)(1-\varepsilon_z)} + k_v\frac{H\varepsilon_z}{2(1-\varepsilon_z)} \tag{17}$$

3. Evaluation Methods

To evaluate the effectiveness of the proposed structure, both experimental and numerical analyses are conducted. For the single SIHA cell, the validity of the mechanical analysis presented above is also revealed. This section introduces the experiment conditions, materials properties, specimen preparation, and simulation settings.

The single unit cell shown in Fig. 2(d) is simulated and tested to catch the performance and negative Poisson's ratio behavior. The dimensional parameters of the SIHA unit cell are as follows: $a = 10$ mm, $H = 12$ mm, $d = 5$mm, and $\theta = \pi/3$. Furthermore, a periodic SIHA structure consisting of 24 unit cells is created to evaluate the mechanical response at a larger scale with a 69 mm side length in all directions. The relatively small number of repeating unit cells is chosen due to the constraint on build size limit of our 3D printer. Although some researchers [44] indicated that the influence of the number of unit cells may be less noticeable compared to that of the structural design, we recognize that size effect may still exist and more number of repeating units would help to further mitigate the size effect.

The CAD model constructed with the twenty-four auxetic hexagonal column unit cells is shown in Fig. 3(a). Also, a conventional 3D re-entrant honeycomb auxetic structure (REH) by referring to Yang et al. [45] is also created for comparison. As shown in Fig. 3(b), the dimension of the REH is kept 69 mm in all directions as well, and the volume of the material is also kept identical to that of SIHA periodic model by altering the wall thickness. Thus, the SIHA and REH models share the same volume density for a fair comparison.

To investigate the mechanical properties of SIHA and REH structures, the commercial FEA software ABAQUS is used to perform the deformation simulation under quasi-static compression conditions. The quasi-static compression speed is controlled at 1mm/s. In the quasi-static study, we adopt a commercial rubber-like photosensitive resin (Tenacious from Siraya Tech), and structures are made by using DLP 3D printing in which the resin is cured by UV light. The mechanical properties of the cured polymer are measured from the standard tensile method (ASTM D638-IV), and the obtained stress-strain curve is shown in Fig. 4. Meanwhile, the mass density is 1178 kg/m^3, Young's modulus is 411.5 MPa, and Poisson's ratio is 0.35 for the DLP printed material. Since friction in the sliding mechanism is an important consideration, the surface contact properties are measured by the standard test method (ASTM D1894). The schematic of such measurement is shown in Fig. 5(a), in which two printed Tenacious resin samples slide against each other under compression loading. A load cell is used to create a horizontal traction force to drive the weight moving forward with the cured resin. Thus, the friction coefficient $\mu = F/P$ can be obtained after the weight moves 150mm forward. Fig. 5(b) shows that the average friction coefficient is approximately 0.64 after relatively stable drag force is reached in the sliding process.

In FEA simulation, elements for both SIHA and REH are linear hexahedral element C3D8R and controlled by the edge size with 1 mm. The meshed single SIHA cell, and periodic SIHA and REH models are shown in Fig. 6. Two rigid plates are created on the top surface and the button

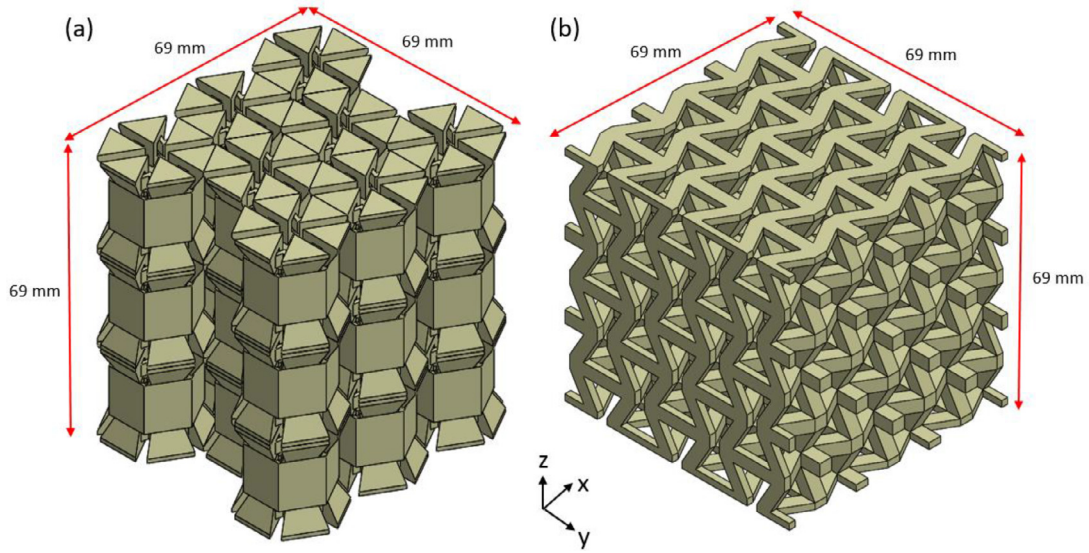

Fig. 3. Constructed models for comparison, (a) the SIHA periodic model, (b) the conventional 3D re-entrant honeycomb auxetic structures REH.

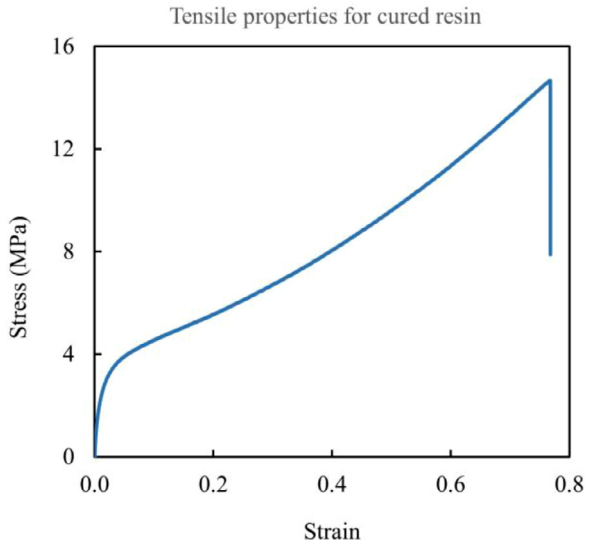

Fig. 4. Stress-strain curve for 3-D printing samples of Siraya Tech Tenacious resin

surface of the mashed model to apply the axial compression load along the *z*-direction. The compression simulation is realized by applying a uniaxial movement along *z* axis for the top rigid plate, while the bottom rigid plate is stationary. The applied uniaxial displacement on the top rigid plate is set to reach 50% strain, at the deformation speed of 1mm/s (which identical to the experimental condition), for all simulation models. Meanwhile, the surface contact is considered in the simulation for all the interactions between surfaces, and the friction coefficient of 0.64 is adopted based on the aforementioned experiment. In the single-cell model, the total number of elements is 7592, while in the periodic SIHA and REH models, the total numbers of elements are 159680 and 119936, respectively. Also, the standard self-contact with the assigned friction coefficient is applied. The deformation pattern and the interaction force between the top rigid plate and the structure models are studied.

The single SIHA unit cell and the periodic SIHA and REH models in Figs. 2 and 3 are realized by DLP 3-D printing. The finished samples of single SIHA cells, and periodic SIHA and REH structures are shown in Fig. 7. They are then tested by a universal material testing system (Model: Shimdzu AGS-X) under compression load. The compression speed is kept at 1 mm/s. The obtained results are then compared with the simulation results.

4. Results and Discussion

In this study, the investigation consists of three major tasks. The first task is about evaluating the performance of the single SIHA unit cell, the second task is about evaluating the performance of the periodic SIHA model and its comparison with the conventional REH structure, and the third task is the sensitivity analysis on the effect of friction condition for the periodic SIHA model. The results on the three tasks are summarized and discussed accordingly.

4.1. Evaluation of collapsing sliding mechanisms in single SIHA unit cell

The influence of collapsing sliding mechanisms is investigated for the single SIHA unit cell under compression load. It can be seen that the compression force of the SIHA cell increases nonlinearly with the strain as shown in Fig. 8(a), where the sliding mechanism is effectively generated by the horizontal collapsing force of the internal supporting structure. This can be used to trap the elastic energy to increase the uniaxial compression force against the sliding surface. The compression force is increased because the collapsing of support structure can provide a higher normal force against the sliding surface. Meanwhile, Fig. 8(b) shows that the negative Poisson's ratio decreases with the increase of the strain, and the SIHA cell exhibits auxetic behavior through the sliding mechanism. The minimum Poisson's ratio of a single unit cell is about -0.3 for both experimental and simulation results. The ideal Poisson's ratio calculated by Eq. (7) shown in Fig. 8(b) indicates that it could reach the minimum of -0.48, which is lower than the experimental and simulation results by a noticeable amount. The discrepancy can be attributed to the following reason. The theoretical model in Eq. (7) only considers the geometry design of the SIHA unit cell, while the deformation properties of the material are not considered. The deformation of the material can affect the sliding mechanism during the compression, resulting in the increase of Poisson's ratio. Thus, the theoretical model can illustrate the maximum performance of the geometry design, and simulation results are more suitable for the real-world scenario. To this end, the simulation results and experimental results of the single unit cell are well agreed. The SIHA unit cell is shown to be effective.

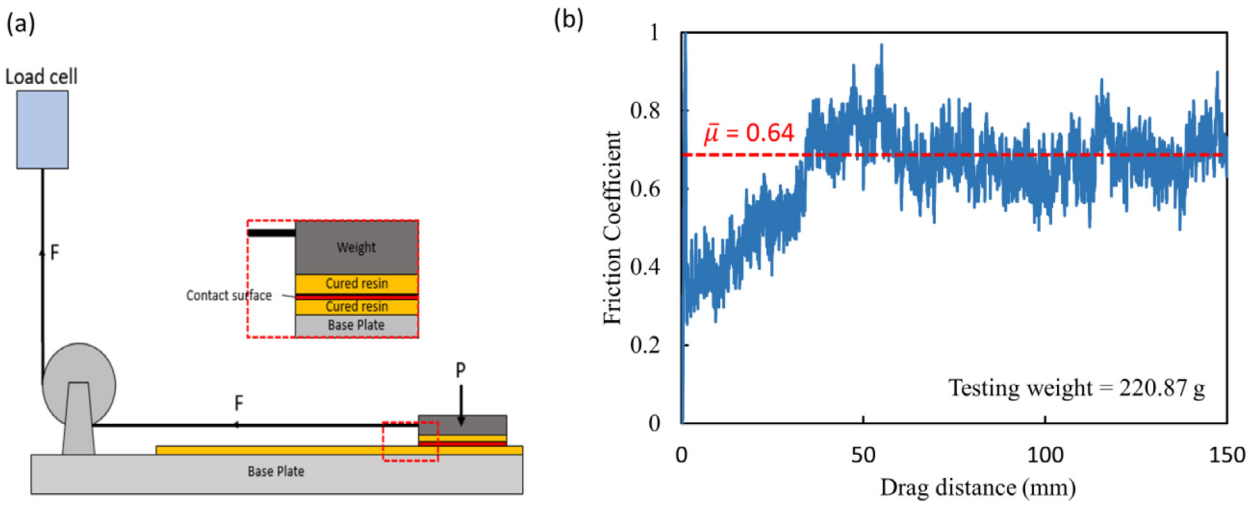

Fig. 5. Friction coefficient measurement for printed polymer materials, (a) schematic of test set-up, (b) the friction coefficient result.

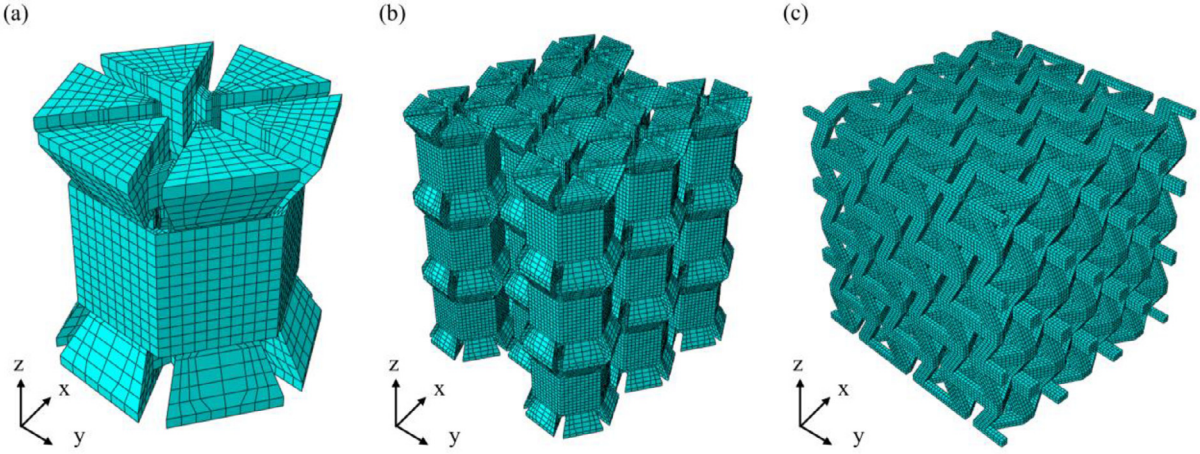

Fig. 6. Schematic diagrams of the meshed models, (a) single SIHA unit cell, (b) periodic SIHA model, and (c) periodic REH model

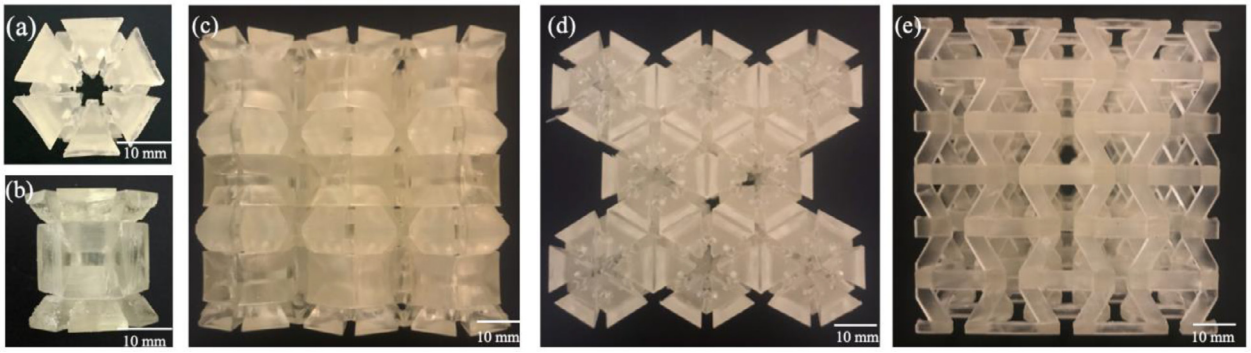

Fig. 7. DLP 3D printed samples, (a) single SIHA unit cell - top view, (b) single SIHA unit cell - side view, (c) periodic SIHA - side view, (d) periodic SIHA - top view, and (e) periodic REH - side view

4.2. Quasi-static compression of periodic SIHA and REH structures

The mechanical behaviors of the periodic SIHA and REH structures are evaluated under compression in both FEA simulation and experiment. The results with progressive uniaxial strain for SIHA structure are shown in Fig. 9(a)-(e), while those for REH are demonstrated in Fig. 9(f)-(j). The deformation patterns for both RSEM and REH structures show good agreement between simulation and experiment. The horizontal dimension shrinks with the uniaxial strain, and the auxetic behavior is observed for both SIHA and REH. The simulation snapshots in Fig. 9 illustrate the magnitude of horizontal displacement, where the red color indicates the node is moved to the positive direction toward the *x*-axis,

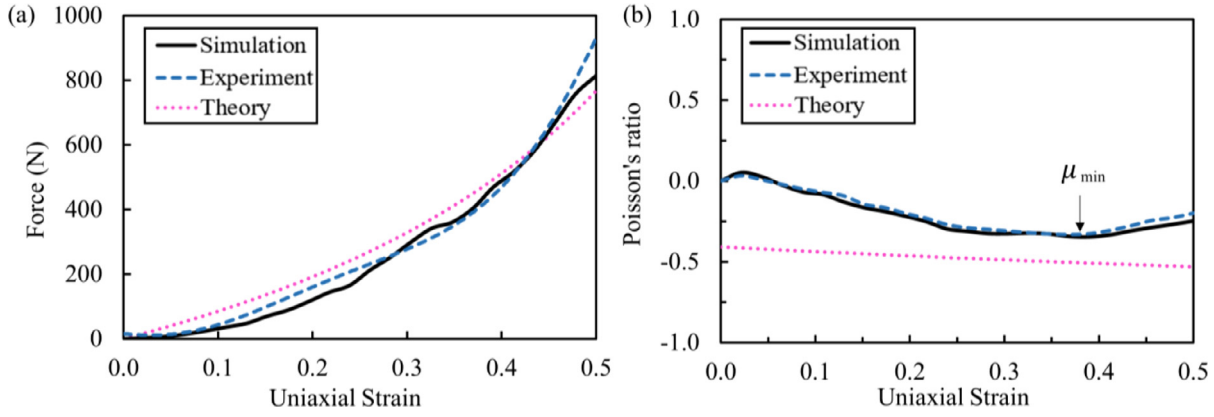

Fig. 8. Performance of single SIHA unit cell, (a) compression force and (b) Poisson's ration with respect to uniaxial strain

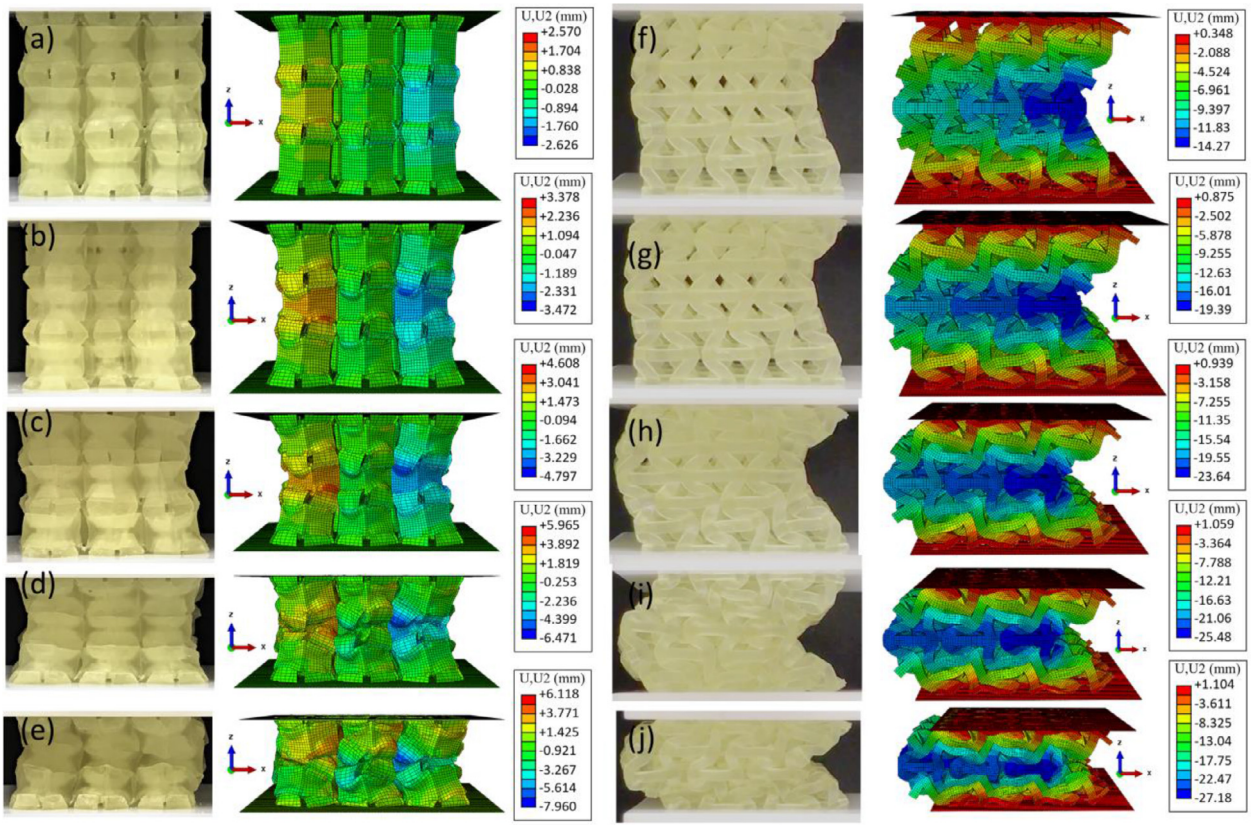

Fig. 9. Compression deformation snapshots in experiment and simulation with various uniaxial strains. (a) SIHA 10% strain, (b) SIHA 20% strain, (c) SIHA 30% strain, (d) SIHA 40% strain, (e) SIHA 50% strain, (f) REH 10% strain, (g) REH 20% strain, (h) REH 30% strain, (i) REH 40% strain, (j) REH 50% strain. (U,U2 = displacement in Y direction)

the blue color indicates the negative displacement along the X-axis, and the green color indicates that the displacement is almost unchanged. The darker the rendered color, the greater the magnitude of displacement.

For the periodic SIHA model, the deformation patterns show the expected results for such design. As it can be seen from Fig. 9(a) and Fig. 9(b), the sliding units start to slide into the hexagonal rings to create horizontal displacement at 10% to 20% uniaxial strain. The maximum magnitude of horizontal displacement is obtained when the uniaxial strain reaches 40% in Fig. 9(d). When the uniaxial strain is over 40%, the SIHA model reaches the densification stage, where the structure has less impact on auxetic behavior [47]. However, the REH structure shows a different deformation pattern. As shown in Fig. 9(f), the buckling occurs when the uniaxial strain is relatively small (less than 10% uniaxial strain). This buckling effect is a common phenomenon when the re-entrant structure is compressed under static loading [12, 24, 45, 48]. However, the REH structure still shows auxetic behavior when the magnitude of horizontal displacement becomes larger in the negative direction, which can be seen in Fig. 9(g) - (i).

The compression forces are extracted and the macroscopic Poisson's ratios for both models are also calculated from simulation and experiment results. The force-strain curves are shown in Fig. 10(a). It can be seen that the results of simulation match with those of experiment very well. Generally, the values obtained from the simulation are slightly higher than the experiment results especially in the early stage of deformation for both SIHA and REH structures. The minor difference could be attributed to the manufacturing imperfections and the friction co-

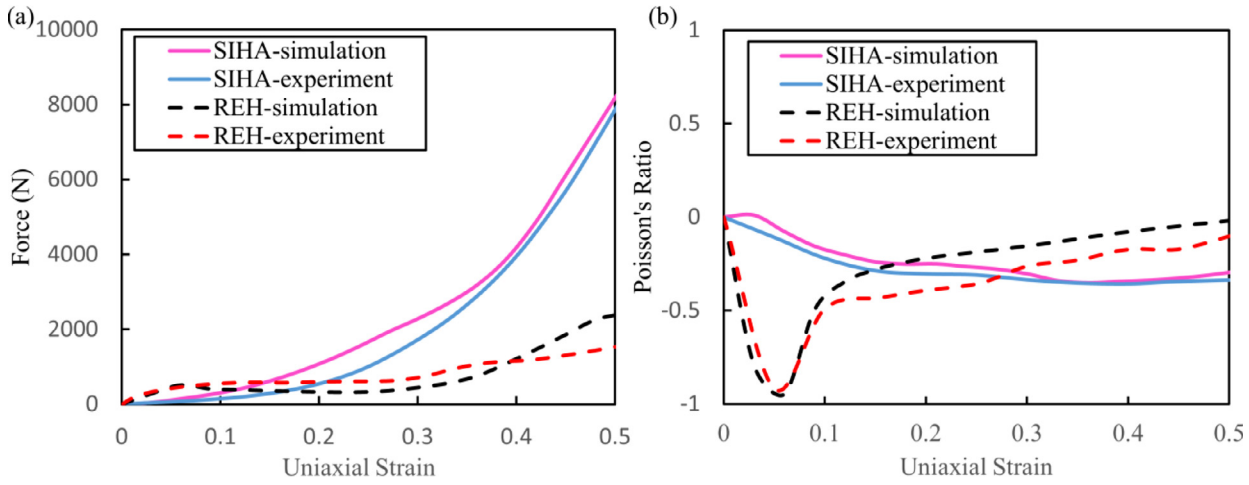

Fig. 10. Experiment and simulation results of SIHA and REH structures, (a) force-strain cures, (b) macroscopic Poisson's ratio-strain curves

efficient variation during the large deformation, which is not easy to control during the experiment [12, 49]. It can be seen that the compression force increases significantly with the compression strain for the SIHA structure, while the increase is less significant for the REH model. The compression force is 8000 N for SIHA when the compression strain reaches 50%, which is approximately four times the REH structure. This is mainly because the significant buckling occurs to the REH structure during the compression. In general, the force-strain curves of SIHA steadily increase because the initial stiffness of the sliding mechanism is relatively low as compared with the conventional REH structure. The low initial stiffness is also observed in other metamaterials with other sliding mechanisms [50, 51]. For the REH structure, the compression force drops in the early stage of deformation, which is related to the same moment when the buckling is observed (8.73%).

Meanwhile, the macroscopic Poisson's ratios for both experiment and simulation results are investigated, as shown in Fig. 10(b). The Poisson's ratio of the SIHA structure appears to steadily decrease during the compression, while that of the REH structure exhibits a more complicated trend, which consists of a rapid initial drop, a quick bounce-back, and then a steady increase, with respect to the increase of strain. This is because the magnitude of horizontal deformation of the sliding mechanism is based on the sliding angle and should be theoretically kept in a constant value, which differs from the re-entrant structure as mentioned in the previous section [30]. The Poisson's ratio curve of the SIHA structure shows that the sliding mechanisms can hold the Poisson's ratio more negative than the REH structure at higher uniaxial strains and relatively stable with the change of strain. The main reason for the phenomenon is because the sliding mechanism does not rotate during the compression. On the other hand, the Poisson's ratio of REH structure changes noticeably due to the frame rotation during the compression, and thus the magnitude of Poisson's ratio change along with the uniaxial strain is higher than that of SIHA, in particular in the initial deformation stage with strain less than 0.1. The observed fluctuation in initial deformation period and overall trend of Poisson's ration for REH structure are highly consistent with literature observations [44, 46, 52], all of which show that the REH structure's Poisson's ratio sharply drops and quickly bounces back before the strain reaches 0.1. Also, in literature, some researchers suggested that a more stable Poisson's ratio can be obtained by adding extra structure to REH [24, 53], but the downside is that the increased strength of the structure will lead to a certain amount of loss in terms of auxetic behavior. For instance, Chen et al. [53] proposed an REH structure with an additional variant to increase the stiffness of REH which could maintain the Poisson's ratio around -0.2, but this is significantly higher than the value of -0.4 for the SIHA structure proposed in this study. As such, compared with the REH structure, the SIHA structure generally reduces Poisson's ratio fluctuation in the initial period of deformation and possesses more negative Poisson's ratio at the higher strain region.

4.3. Sensitivity of friction coefficient

The mechanical behavior of SIHA is controlled by the moving of sliding units, where friction plays a very important role. To exam the influence of friction conditions on the quasi-static performance of the SIHA structure, scenarios with various friction coefficients are simulated. The input friction coefficient varies at 0.1, 0.3, 0.5, and 0.7, respectively. The deformation snapshots at the strain deformation of I 0%, II 12.5%, III 25%, IV 37.5%, V 50%, respectively for those scenarios are shown in Fig. 11. The results show that the friction coefficient has significant effect on the deformation of the SIHA structure. When low friction is applied, the buckling occurs because there is insufficient friction force to balance uneven stress created by the deformation and contact within the structure. The SIHA shows the desired deformation pattern when the friction coefficient reaches 0.3. However, when the friction coefficient exceeds 0.5, the sliding surface begins to deform before the sliding units slide into the structure, which is shown in the highlighted areas III with 25% strain in Fig. 11 (c) and (d). Furthermore, in the case of friction coefficient 0.7, the sliding mechanism largely fails because of the friction force-intensive buckling effect in the middle layer.

The force-strain curves of the simulation scenarios with different applied friction coefficients are extracted and shown in Fig. 12(a). In general, the average force value increases with the applied friction coefficient because the friction force can provide extra resistance during the compression and offset the uneven force during sliding, which matches the simulation work of Alomarah et al. [49]. When μ=0.7, the sliding behavior barely exists in the structure and buckling occurs because there is sufficient friction force to balance uneven stress created by the deformation and contact within the structure. Meanwhile, the effect of friction coefficient on Poisson's ratio of periodic SIHA is shown in Fig. 12(b). It can be seen that Poisson's ratio of the periodic SIHA structure generally increases with the friction coefficient except for the lowest friction coefficient of 0.1. The Poisson's ratio at μ=0.1 is higher compared with the case of μ=0.3 because the very low friction condition causes the uneven buckling to the sliding mechanism. Meanwhile, in the high friction condition, the friction force causes insufficient sliding in the structure, which can in turn cause localized buckling instabilities and then expand to a larger area, which is also reported by Hu et al. [54]. As such, the performance of periodic SIHA structure based on the sliding mechanism is sensitive to the friction force at quasi-static load. The friction condi-

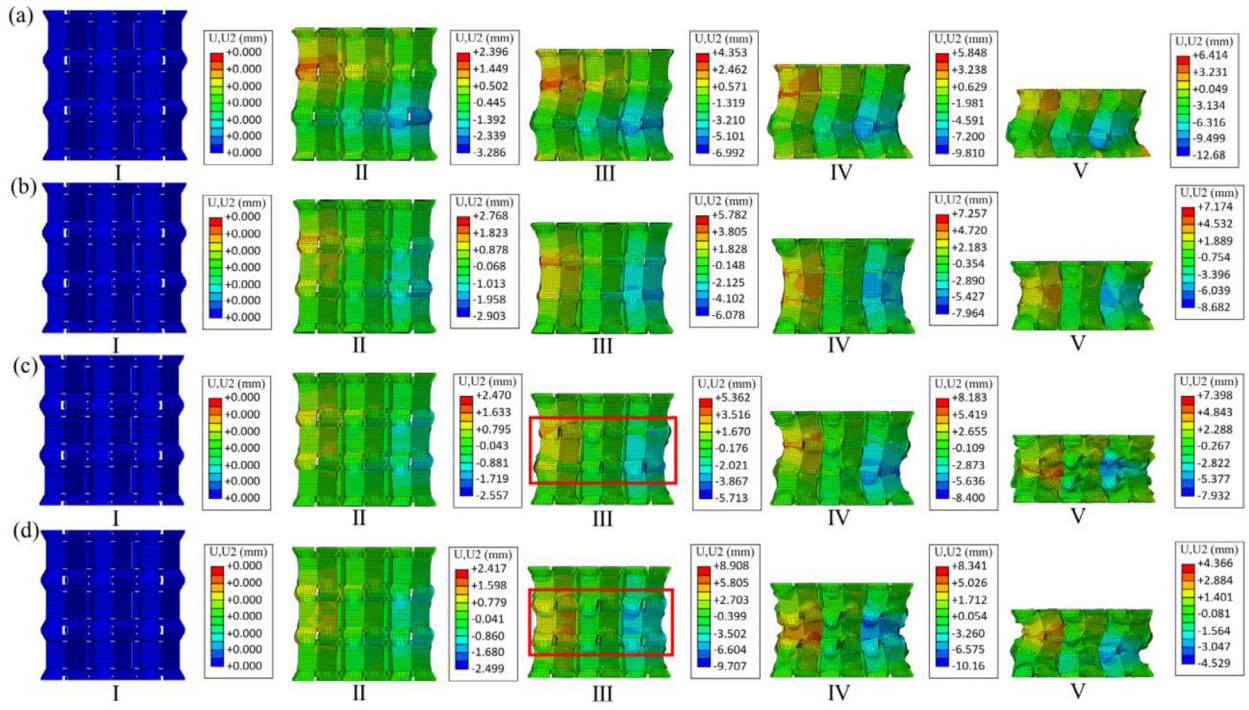

Fig. 11. Deformation pattern of SIHA with friction coefficients from (a) μ = 0.1, (b) μ = 0.3, (c) μ = 0.5, (d) μ = 0.7 and from I to V with strain deformation 0%, 12.5%, 25%, 37.5%, 50%, respectively. (U,U2 = displacement in Y direction)

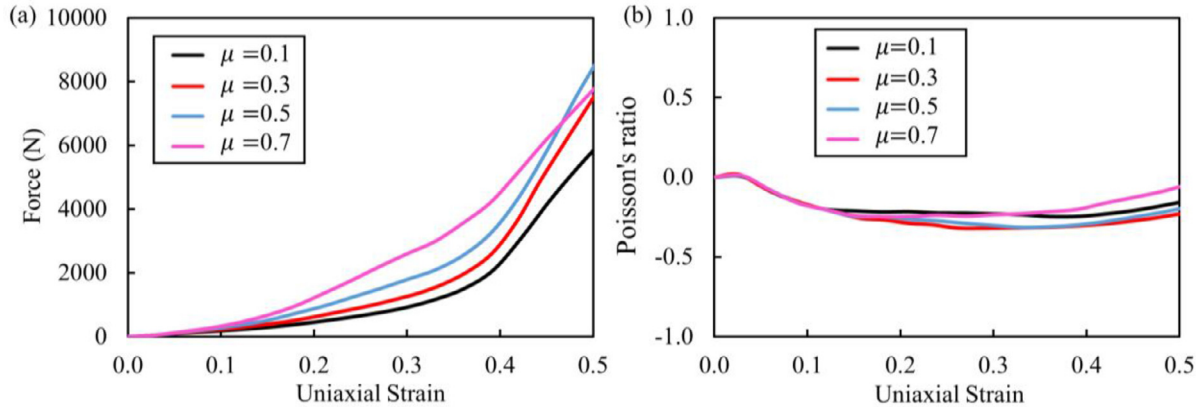

Fig. 12. Effect of friction coefficient on the performance of SIHA metamaterial, (a) force-strain curves, and (b) Poisson's ratio versus strain with friction coefficients of 0.1-0.7.

tion should be one of the main control parameters to be considered in designing such metamaterials.

5. Conclusions

In this study, we propose a novel sliding induced hexagonal auxetic (SIHA) metamaterial inspired by the conventional hexagonal structure and the sliding auxetic structure. The unique design of the sliding units employs a sliding mechanism that generates the auxetic behavior. Meanwhile, the embedded collapsing mechanisms could be used to trap energy with guaranteed negative Poisson's ratio under uniaxial compression.

The single cell of the SIHA design is evaluated by mechanical analysis, FEA simulation, and experiment verification. Satisfactory agreement is achieved among the three approaches. Moreover, the performance of the periodic SIHA structure is evaluated and compared with the classic periodic REH structure. It is again found that the FEA simulation results are overall consistent with the experiment. A noticeable improvement of mechanical properties over the conventional REH structure is demonstrated – the results show that the proposed SIHA structure could incur compression force four times that of the REH structure under quasi-static compression loading, and a more stable auxetic behavior in the initial deformation period is observed with the SIHA structure. Furthermore, the contact surface friction condition is demonstrated to be an important parameter to control the sliding auxetic behavior.

In brief, the sliding mechanism in the geometry design successfully introduces a new type of auxetic metamaterials which has the potential to improve the common weak points of conventional auxetic metamaterials such as high Poisson's ratio and low strength under large deformation. The principles and design performance of the SIHA structure are verified by experiment and simulation. On the other hand, the current research should be regarded as a starting point for the promising metamaterial structure. Extension work is expected to be conducted in the future. For instance, optimal design of the structure should be addressed

such that weight reduction under the constraint of manufacturing capability can be achieved. Also, the energy absorption capability should be further evaluated so that a relatively flat force to stroke curve can be achieved under impact loading.

Declaration of competing interest

The authors declare that they have no known competing financial interests or personal relationships that could have appeared to influence the work reported in this paper.

CRediT authorship contribution statement

Yutai Su: Investigation, Visualization, Data curation, Formal analysis, Writing – original draft, Writing – review & editing. **Xianchen Xu:** Investigation, Writing – original draft. **Jing Shi:** Conceptualization, Supervision, Writing – original draft, Writing – review & editing. **Guoliang Huang:** Methodology, Supervision.

Acknowledgments

J.S. acknowledges that the research was partly supported by a grant from the National Science Foundation (CMMI# 1563002). G.H. acknowledges the funding support by the NSF CMMI under award no. 1930873.

References

[1] Kshetrimayum R. A brief intro to metamaterials. IEEE Potentials 2005;23:44–6. doi:10.1109/mp.2005.1368916.
[2] Tanaka T, Ishikawa A, Kawata S. Unattenuated light transmission through the interface between two materials with different indices of refraction using magnetic metamaterials. Physical Review B 2006;12:125423. doi:10.1103/PhysRevB.73.125423.
[3] Xu X, Li P, Zhou X, Hu G. Experimental study on acoustic subwavelength imaging based on zero-mass metamaterials. EPL (Europhysics Letters) 2015;2:28001. doi:10.1209/0295-5075/109/28001.
[4] Osman M, Shazly M, El-Danaf E, Jamshidi P, Attallah M. Compressive behavior of stretched and composite microlattice metamaterial for energy absorption applications. Composites Part B: Engineering 2020;184:107715. doi:10.1016/j.compositesb.2019.107715.
[5] Wu X, Su Y, Shi J. Perspective of additive manufacturing for metamaterials development. Smart Materials and Structures 2019;28:093001. doi:10.1088/1361-665x/ab2eb6.
[6] Iyer A, Eleftheriades G. Negative refractive index metamaterials supporting 2-D waves. 2002 IEEE MTT-S International Microwave Symposium Digest (Cat. No.02CH37278 Seattle, WA, USA; 2-7 June 2002. doi:101109/mwsym20021011823.
[7] Zhang S, Fan W, Panoiu N, Malloy K, Osgood R, Brueck S. Experimental demonstration of near-infrared negative-index metamaterials. Physical Review Letters 2005;95:137404. doi:10.1103/physrevlett.95.137404.
[8] Cummer SA, Schurig D. One path to acoustic cloaking. New Journal of Physics 2007;3:45. doi:10.1088/1367-2630/9/3/045.
[9] Xu X, Wang C, Shou W, Du Z, Chen Y, Li B, Matusik W, Hussein N, Huang G. Physical realization of elastic cloaking with a polar material. Physical Review Letters 2020;11:114301. doi:10.1103/PhysRevLett.124.114301.
[10] Hart W, Bak A, Phillips C. Ultra low-loss super-resolution with extremely anisotropic semiconductor metamaterials. AIP Advances 2018;8:025203. doi:10.1063/1.5013084.
[11] Bertoldi K, Vitelli V, Christensen J, Hecke MV. Flexible mechanical metamaterials. Nature Reviews Materials 2017;11:1–11 doi.org/. doi:10.1038/natrevmats.2017.66.
[12] Frenzel T, Kadic M, Wegener M. Three-dimensional mechanical metamaterials with a twist. Science 2017;6366:1072–4. doi:10.1126/science.aao4640.
[13] Ren X, Das R, Tran P, Ngo T, Xie Y. Auxetic metamaterials and structures: a review. Smart Materials and Structures 2018;27:023001. doi:10.1088/1361-665x/aaa61c.
[14] Lakes R. Foam Structures with a Negative Poisson's Ratio. Science 1987;235:1038–40. doi:10.1126/science.235.4792.1038.
[15] Gibson L, Ashby M, Harley B. Cellular materials in nature and medicine. Cambridge: Cambridge University Press; 2010.
[16] Masters I, Evans K. Models for the elastic deformation of honeycombs. Composite Structures 1996;35:403–22. doi:10.1016/s0263-8223(96)00054-2.
[17] Wang T, Li Z, Wang L, Ma Z, Hulbert G. Dynamic crushing analysis of a three-dimensional re-entrant auxetic cellular structure. Materials 2019;12:460. doi:10.3390/ma12030460.
[18] Li T, Hu X, Chen Y, Wang L. Harnessing out-of-plane deformation to design 3D architected lattice metamaterials with tunable Poisson's ratio. Scientific Reports 2017;7. doi:10.1038/s41598-017-09218-w.
[19] Yuan S, Chua C, Zhou K. 3D-printed mechanical metamaterials with high energy absorption. Advanced Materials Technologies 2018;4:1800419.
[20] Dagdelen J, Montoya J, de Jong M, Persson K. Computational prediction of new auxetic materials. Nature Communications 2017;8:323. doi:10.1038/s41467-017-00399-6.
[21] Saxena K, Das R, Calius E. Three decades of auxetics research – Materials with negative Poisson's ratio: A review. Advanced Engineering Materials 2016;18:1847–70. doi:10.1002/adem.201600053.
[22] Li X, Wang Q, Yang Z, Lu Z. Novel auxetic structures with enhanced mechanical properties. Extreme Mechanics Letters 2019;27:59–65. doi:10.1016/j.eml.2019.01.002.
[23] Meena K, Singamneni S. A new auxetic structure with significantly reduced stress concentration effects. Materials & Design 2019;173:107779. doi:10.1016/j.matdes.2019.107779.
[24] Su Y, Wu X, Shi J. A novel 3D printable multimaterial auxetic metamaterial with reinforced structure: Improved stiffness and retained auxetic behavior. Mechanics of Advanced Materials and Structures 2020:1–11. doi:10.1080/15376494.2020.1774690.
[25] Chen J, Chen W, Hao H, Huan S, Tao W. Mechanical behaviors of 3D re-entrant honeycomb polyamide structure under compression. Materials Today Communications 2020;24:101062. doi:10.1016/j.mtcomm.2020.101062.
[26] X. Zhang, R. Tian, Z. Zhang, G. Li, W. Feng, In-plane elasticity of a novel vertical strut combined re-entrant honeycomb structure with negative Poisson's ratio, Thin-Walled Structures 163 (2021) 107634. doi:10.1016/j.tws.2021.107634.
[27] Yang H, Ma L. Design and characterization of axisymmetric auxetic metamaterials. Composite Structures 2020;249:112560. doi:10.1016/j.compstruct.2020.112560.
[28] Ai L, Gao X. Three-dimensional metamaterials with a negative Poisson's ratio and a non-positive coefficient of thermal expansion. International Journal of Mechanical Sciences 2018;135:101–13. doi:10.1016/j.ijmecsci.2017.10.042.
[29] Chen Y, Fu M. A novel three-dimensional auxetic lattice meta-material with enhanced stiffness. Smart Materials and Structures 2017;26:105029. doi:10.1088/1361-665x/aa819e.
[30] Kim J, Shin D, Lee S, Lee J, Kwon S, Yoon S, Yoo D, Kim K. Auxetic structures with regularly configured rigid sliding units. Physica Status Solidi (B) 2017;254:1600335. doi:10.1002/pssb.201600335.
[31] Lim T. Metamaterials with Poisson's ratio sign toggling by means of microstructural duality. SN Applied Sciences 2019;1. doi:10.1007/s42452-019-0185-1.
[32] Hewage T, Alderson K, Alderson A, Scarpa F. Double-negative mechanical metamaterials displaying simultaneous negative stiffness and negative Poisson's ratio properties. Advanced Materials 2016;28:10323–32. doi:10.1002/adma.201603959.
[33] Ren X, Shen J, Tran P, Ngo T, Xie Y. Design and characterisation of a tuneable 3D buckling-induced auxetic metamaterial. Materials & Design 2018;139:336–42. doi:10.1016/j.matdes.2017.11.025.
[34] Xu X, Zhang Y, Wang J, Jiang F, Wang C. Crashworthiness design of novel hierarchical hexagonal columns. Composite Structures 2018;194:36–48. doi:10.1016/j.compstruct.2018.03.099.
[35] Reid S, Harrigan J. Transient effects in the quasi-static and dynamic internal inversion and nosing of metal tubes. International Journal of Mechanical Sciences 1998;40:263–80. doi:10.1016/s0020-7403(97)00054-4.
[36] Niknejad A, Moeinifard M. Theoretical and experimental studies of the external inversion process in the circular metal tubes. Materials & Design 2012;40:324–30. doi:10.1016/j.matdes.2012.04.005.
[37] Qiu X, He L, Gu J, Yu X. An improved theoretical model of a metal tube under free external inversion. Thin-Walled Structures 2014;80:32–7. doi:10.1016/j.tws.2014.02.025.
[38] Li J, Gao G, Dong H, Xie S, Guan W. Study on the energy absorption of the expanding–splitting circular tube by experimental investigations and numerical simulations. Thin-Walled Structures 2016;103:105–14. doi:10.1016/j.tws.2016.01.031.
[39] Thomas T, Tiwari G. Crushing behavior of honeycomb structure: a review. International Journal of Crashworthiness 2019;24:555–79. doi:10.1080/13588265.2018.1480471.
[40] Pullar R. Hexagonal ferrites: A review of the synthesis, properties and applications of hexaferrite ceramics. Progress in Materials Science 2012;57:1191–334. doi:10.1016/j.pmatsci.2012.04.001.
[41] Tarlochan F, Faridz A. Sustainability design: Reduction of vehicle mass without compromizing crashworthiness. 2009 3rd International Conference on Energy and Environment (ICEE) Malacca, Malaysia; 7-8 Dec. 2009. doi:101109/iceenviron20095398620.
[42] Ajdari A, Nayeb-Hashemi H, Vaziri A. Dynamic crushing and energy absorption of regular, irregular and functionally graded cellular structures. International Journal of Solids and Structures 2011;48:506–16. doi:10.1016/j.ijsolstr.2010.10.018.
[43] Nakamoto H, Adachi T, Araki W. In-plane impact behavior of honeycomb structures randomly filled with rigid inclusions. International Journal of Impact Engineering 2009;36:73–80. doi:10.1016/j.ijimpeng.2008.04.004.
[44] R. Yu, W. Luo, H. Yuan, J. Liu, W. He, Z. Yu, Experimental and numerical research on foam filled re-entrant cellular structure with negative Poisson's ratio, Thin-Walled Structures 153 (2020) 106679. doi:10.1016/j.tws.2020.106679.
[45] Yang L, Harrysson O, West H, Cormier D. Mechanical properties of 3D re-entrant honeycomb auxetic structures realized via additive manufacturing. International Journal of Solids and Structures 2015;69:475–90. doi:10.1016/j.ijsolstr.2015.05.005.
[46] Dong Z, Li Y, Zhao T, Wu W, Xiao D, Liang J. Experimental and numerical studies on the compressive mechanical properties of the metallic auxetic reentrant honeycomb. Materials & Design 2019;182:108036. doi:10.1016/j.matdes.2019.108036.
[47] Ghaedizadeh A, Shen J, Ren X, Xie Y. Tuning the performance of metallic auxetic metamaterials by using buckling and plasticity. Materials 2016;9:54. doi:10.3390/ma9010054.

[48] Wu X, Su Y, Shi J. In-plane impact resistance enhancement with a graded cell-wall angle design for auxetic metamaterials. Composite Structures 2020;247:112451. doi:10.1016/j.compstruct.2020.112451.
[49] A. Alomarah, S. Masood, I. Sbarski, B. Faisal, Z. Gao, D. Ruan, Compressive properties of 3D printed auxetic structures: experimental and numerical studies, Virtual and Physical Prototyping 15 (2019) 1-21. doi:10.1080/17452759.2019.1644184.
[50] Bodaghi M, Liao WH. 4D printed tunable mechanical metamaterials with shape memory operations. Smart Materials and Structures 2019;28(4):045019. doi:10.1088/1361-665X/ab0b6b.
[51] Tan X, Wang B, Yao K, Zhu S, Chen S, Xu P, Sun Y. Novel multi-stable mechanical metamaterials for trapping energy through shear deformation. International Journal of Mechanical Sciences 2019;164:105168. doi:10.1016/j.ijmecsci.2019.105168.
[52] Wang H, Lu Z, Yang Z, Li X. A novel re-entrant auxetic honeycomb with enhanced in-plane impact resistance. Composite Structures 2019;208:758–70. doi:10.1016/j.compstruct.2018.10.024.
[53] Chen Z, Wu X, Xie Y, Wang Z, Zhou S. Re-entrant auxetic lattices with enhanced stiffness: A numerical study. International Journal of Mechanical Sciences 2020;178:105619. doi:10.1016/j.ijmecsci.2020.105619.
[54] Hu J, Zhou Y, Liu Z. The friction effect on buckling behavior of cellular structures under axial load. International Journal of Applied Mechanics 2018;10:1850013. doi:10.1142/s1758825118500138.